ISME

Dynamic Modelling of a Compressed Air Energy Storage System in a Grid Connected Photovoltaic Plant

A. Arabkoohsar*
PhD

M. Farzaneh-Gord†
Professor

R.N.N. Koury‡
Professor

The use of photovoltaic (PV) cells in domestic and industrial applications has grown rapidly through the recent years. Constructing PV plants is a very smart measure to produce free electricity in large scales, especially in the countries with higher solar irradiation potential. On the other hand, compressed air energy storage (CAES) has already been proposed to be employed for energy storage applications. In this work, erecting a large scale grid connected PV plant accompanying with a CAES system to produce either all (if applicable) or a portion of the required electricity, in the most appropriate geographical location in Brazil, is proposed. In the first step, the best point for erecting the power plant is chosen regarding climate and solar engineering considerations. Then, the best tracking mode for the PV cells is opted based on energy and economic considerations. The CAES system is designed and analyzed in the next step. In order to prove the proficiency of the proposal, the performance of the PV plant as well as the CAES unit is assessed for a whole year in the chosen city.

Keywords: PV Plant, Tracker, CAES, Energy Analysis

1 Introduction

Among all renewable energy sources, the sun is the most plentiful and available. The radiated energy from the sun is 3.8×10^{23} kW, of which, almost 1.8×10^{14} kW is received by the earth. This amount of energy is almost well above 7500 times the world's total annual energy demand [1]. In PV technologies, sunlight is directly converted into electricity by striking PV panels which contain no moving parts [2]. PV panels can generate electricity employing the sun clean energy; therefore, they are environmentally friendly. Furthermore, low restriction in installation location and low maintenance costs are other advantages of such panels [3].
PV panels can be employed in both small and large electricity production scales. In small scale, they can be individually installed on the houses roofs for reducing or even eliminate electricity bills. This application of PV panels is even much more impressing for the places that are far away from the electricity distribution grids.

*Corresponding Author, PhD, Department of Mechanical Engineering, Azadshahr Branch, Islamic Azad University, Azadshahr, Iran, mani.koohsar@yahoo.com
†Professor, Department of Mechanical Engineering, Shahrood University of Technology, Shahrood, Iran, mahmood.farzaneh@yahoo.co.uk
‡Professor, Department of Mechanical Engineering, Federal University of Minas Gerais (UFMG), BH, Brazil, Koury@ufmg.br

In large scale, on the other hand, large PV farms can be built to provide the required electricity of cities, big factories and so on [4]. The first 1 MW_p (peak power capacity) PV farm was built in California in (1982), then in (1984), the second plant with a capacity of 5.2 MW_p in Carrizo Plain was constructed [5]. Thereafter, many others were installed in various points all round the world one after another. By (2013), the installed PV power around the world is close to 139 GWp and only 38 GWp in Germany as the biggest host of such technology throughout the world [6]. The capacity of solar farms can vary from only 1 MWp up to hundreds of MWp. Agua Caliente is the largest in operation PV plant in the world with a capacity of 290 MWp in Arizona [7].

The main problems of renewable energy power plants (specifically PV plants here) is that the source of energy is inherently intermittent. Therefore, instantaneous variations of electricity demand in the grid could not be accurately responded [8]. For overcoming this problem in a PV plant, firstly, unpredictable and steep ramps in the electricity demand of grid, and secondly, the ramps in local solar irradiation should be taken into account. Therefore, accurate forecast would eliminate these problems entirely [9]. As accurate prediction of these two parameters is not achievable practically; the best solution seems to be employing energy storage systems and reclaiming the stored energy by the time of demand [10]. Various energy storage systems have already been proposed in the literature.

Battery, flywheel, capacitor, pumped hydroelectric energy storage (PHES), super conducting magnetic energy storage (SMES), cryogenic energy storage (CES) and compressed air energy storage (CAES) are the most efficient systems proposed ever [11]. For large scale storage capacities, PHES and CAES are the most promising systems, though PHES has certain adverse environmental effects [12]. Comparing with all the aforementioned storage technologies, CAES has a lower capital and maintenance cost and is also totally environmentally friendly. That's why CAES system has attracted more attention in the recent times [13]. To the extent of the authors' knowledge, no detailed assessment on a PV plant equipped with a CAES system in real case has been reported in the literature yet, though there are many renewable energy electricity production plants as well as a few CAES systems along with conventional power plants working separately. On the other hand, in spite of great solar energy potential, not many grid connected PV farm has been installed in Brazil by now, though a few more PV plants are supposed to be run in small capacities shortly. The largest in operation PV plant in Brazil has an installed capacity of 3 MWp and made up of 19,424 panels in the city of Tuberão [14]. A bigger plant is also going to be installed with a capacity of 8.5 MWp in Luziania [15]. All in operation solar power plants in this country are equipped with traditional storage systems i.e. batteries. In this work, installing the largest PV plant of Brazil which is equipped with a large enough and efficient CAES unit for a city which is the most appropriate point in terms of weather condition and the amount of solar irradiation all over the country is proposed. The performance of the power plant through a whole year (as a sample year of operation) is assessed and detailed energy analysis on the power plant and the CAES system is presented.

2 PV Farm

For constructing a PV plant, there are some important issues to be assessed in the design stage. First of all, the best location for constructing the plant should be defined, regarding the weather, climate and geographical considerations. Clearly, the best place for constructing a solar power plant is the point that receives maximum solar irradiation and has the least cloudy and rainy hours over the year. As there is no guarantee the maximum solar irradiation receiver point has also the clearest sky all around the country, therefore, one should trade off to specify the pest location of the plant.

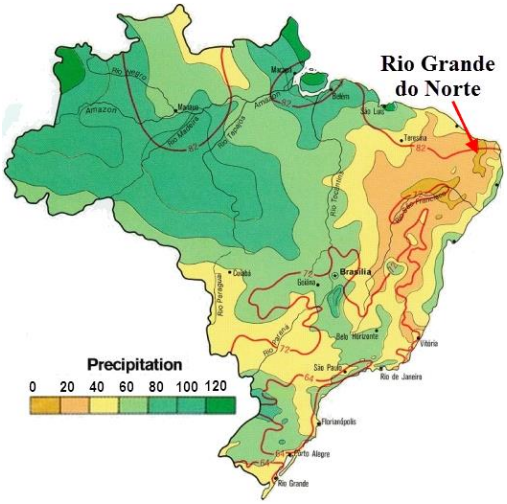

Figure 1 Brazil's precipitation map

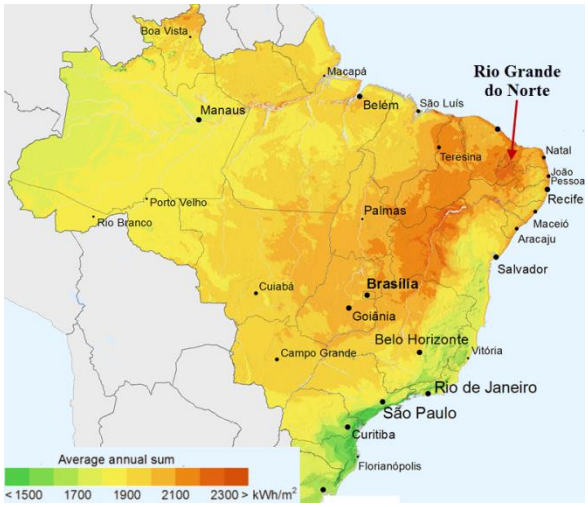

Figure 2 Brazil's normal solar irradiation intensity map

Precipitation map is used to compare the sky clarity in various locations through Brazil. Figure (1) shows the map of average annual precipitation in Brazil [16].
Figure (2) also shows solar irradiation intensity map throughout Brazil [16].
According to the figures, the west and middle area of Rio Grande do Norte state (Caico city) is the best point for construction a PV farm. Therefore, this area can be opted as one of the most suitable places to host a solar power plant. There are various methodologies for calculating the amount of available solar irradiation. The total hourly solar radiation on a horizontal surface beyond the atmosphere (I_o) and on the earth's surface, based on clear sky model, can be calculated employing the following equations [17, 18].

$$I_o = \frac{12\times 3600}{\pi}\cdot G_{sc}\left(1+0.033\cos\frac{360\,n}{365}\right)\left[\cos\varphi\cos\delta\left(\sin\omega_2-\sin\omega_1\right)+\frac{\pi\left(\omega_2-\omega_1\right)}{180}\times\sin\varphi\sin\delta\right] \quad (1)$$

$$I = I_o \times K_T$$

Where, φ is local latitude angle (6.45°), δ is the inclination angle of the sun, n is the number of the day in the year, ω_1 and ω_2 represent the hourly angles related to the beginning and end of hourly periods and G_{sc} is solar constant with the value of 1367 W/m^2. K_T is also the sky clearness index during the hourly period. For calculating the sky clearness index value of Caico, Angstrom coefficients, which are available for all cities in Brazil in [19], could be

used. Note that due to the abundance of references in this area, no more explanation is presented in this work [20-22].

Then, the selection of PV cell that are supposed to be installed for collection of solar irradiation is done. The PV panel (cell) is the main part of a PV system. A PV cell consists of two or more thin layers of semiconducting material, most commonly silicon. When the silicon exposed to light, electrical charges are generated and this can be conducted away by metal contacts as direct current. In fact, based on the conception, a PV cell is composed of a P-type and an N-type semiconductor. Solar irradiation hitting the cell produces two types of electrons, negatively and positively charged electrons in the semiconductors. Negatively charged electrons gather around the N-type semiconductor while positively charged electrons gather around the P-type semiconductor. Upon connecting loads, electric current flows between the two electrodes [23].

Figure (3) shows the schematic diagram of a PV cell. Any number of panels can be added to an existing system as required and normally for a large PV plant depending on the size from thousands to millions of cells should be connected to provide the required electricity amount. Efficiency is an important measure of PV cells that is defined as the maximum electrical power output divided by the incident light power. There are various types of PV cells available each of which has different efficiency and price. Table (1) details information about different types of photovoltaic cells and corresponding maximum efficiencies. Overall, considering the price and efficiency, it is recommended to use monocrystalline silicon cells as the most appropriate type of PV cell for constructing a PV plant [24].

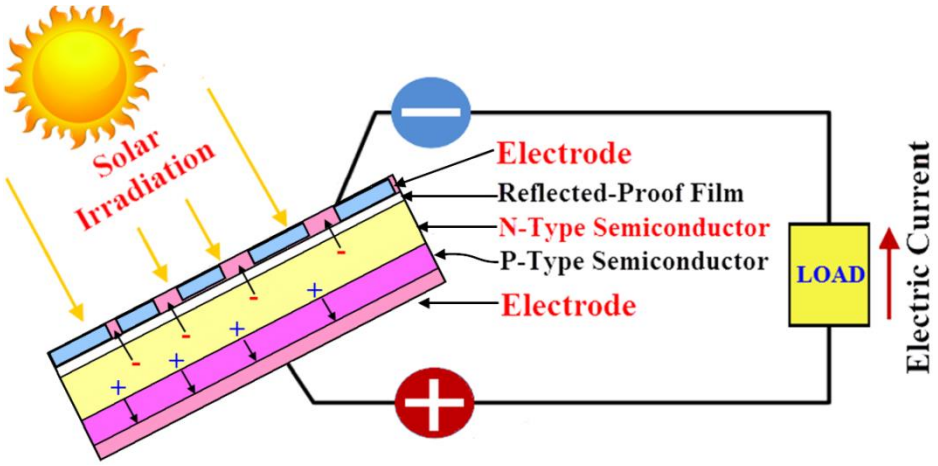

Figure 3 The schematic diagram of a PV cell

Table 1 Details of various PV cells available in the market

Cluster	Type	Expected Efficiency (%)
Silicon Semiconductor	Monocrystalline	15-20
	Multicrystalline	10-14
	Amorphous	7-9
Compound Semiconductor	Gallium Arsenide	19-22
Organic Semiconductor	Dye-sensitized	6-8
	Organic Thin Layer	2-3

The type of employed tracker technology is also necessary to be chosen in the next step, considering energy-economic aspects of the project. After selecting the PV cell type, one should select the best tracking system to maximize the amount of receivable solar irradiation. For this purpose, there are various choices such as employing slopped fixed cells, slopped cells rotating around a vertical axis, cells rotating around the east-west axis with single daily adjustment or with continuous adjustment, the north-south axis rotator planes with continuous adjustment, the north-south axis parallel to the earth's axis rotator cells with continuous adjustment and dual axis rotating cells. In all of these tracking modes, instead of being horizontal, considering the mode of tracking, the cells are inclined and have different angles in different directions. Overall, the amount of solar irradiation on an inclined cell with 1 m^2 area can be given by:

$$I_T = I_b R_b + I_d\left(\frac{1+\cos\beta}{2}\right) + I\cdot\rho_g\left(\frac{1-\cos\beta}{2}\right) \quad (2)$$

Where, I_b, I_d, ρ_g and β are the beam and diffuse components of solar radiation, the sunlight reflection coefficient and the slop angle, respectively. R_b is also a functional of incident angle (the angle between the sunlight and the cell surface, θ). It should be noted that although equation 2 could be used for calculating the amount of receivable solar energy by the cells with all the tracking modes, however, the slop angle (β) and the incident angle (θ) for each case are different and calculated by various equations. As it will be explained in the results section, the performance of north-south axis parallel to the earth's axis sun tracker is the best among all possible tracking modes and as a result, this tracking mode has been selected to be used in the PV farm. The incident angle and the instantaneous slop angle for such a tracking surface could be given as:

$$R_b = \frac{\cos\theta}{\cos\theta_z};\quad \theta = \delta;\quad \beta = \tan^{-1}\left(\frac{\tan\varphi}{\cos\gamma}\right) \quad (3)$$

Where, γ is the surface azimuth angle. In this section also, as many references are available in the literature, more explanation and formulation is abstained [25, 26].

The power production capacity of the plant should also be specified in the next step. This undoubtedly depends on the investor budget and investment plan as well as the total local required electricity. As Rio Grande do Norte population exceeds 3.4 million, there is no restriction for the amount of required electricity. Therefore, as a sample case, a PV plant with a daily averaged electricity production capacity of 50 MW is proposed to be built. Finally, the plant must specify how much electricity will sell to the grid over the year.

3 The CAES System

As solar irradiation intensity is severely intermittent and variable, the existent of an energy storage unit along with the PV plant seems to be inevitable. Therefore, the off peak extra power produced can be stored and then, it could be reclaimed to produce power in either peak consumption hours or intensive solar energy ramps times. Batteries are the first option to be used in PV plants, however, for large scale PV farms; batteries cannot be the best choice due to the very large size of batteries required, limited capacity and some technical problems such as internal self-discharge [27]. The CAES system is one of the most efficient and feasible systems for large scale energy storage purposes [12]. In comparison with PV technology, it is not so long that the CAES technology has been introduced to the industry and as a result, it is still in development stage.

The CAES technology was extensively investigated in the (1970s) to provide load following services and to gain a high capacity factor for base load power plants (especially nuclear) by storing off-peak electricity [13]. The first CAES plant was commissioned in Huntorf, Germany in (1978) to provide peak power for a gas turbine plant. The Huntorf plant, which is still in operation, stores up to 310,000 m^3 of compressed air at a pressure range of 44–70 bar in two salt caverns and can produce up to 290 MW of electricity at full capacity for 4h at an air discharge flow rate of 417 kg/s [27]. The second utility scale CAES plant was also commissioned in (1991) in McIntosh, capable to generate 110 MW of electricity at full capacity for 26h with an air discharge rate of 154 kg/s. It stores up to 540,000 m^3 of compressed air at a pressure range of 45-74 bars in a salt cavern [28]. Unfortunately, in spite of great performance experienced in the aforementioned sites, no more CAES system has gone into commercial operation yet.

(a) CAES Configuration

The first configuration proposed for a CAES system was much simpler than those proposed recently [29]. In the first configuration, the system only took advantage of a single compressor, a single expander and an air storage tank. In the next proposed system, a thermal energy storage tank was added to the first configuration to store the air heat generated through the compression process [30]. This heat could be employed to warm up the air stream in expansion times; therefore, the amount of heat provided by ancillary heaters could decrease significantly. Employing multiple stage compressors and expansions instead of single stage units in the CAES system was the next modification in the system [31]. Finally, adding another heat storage tank made the CAES an efficient energy storage system [32]. Figure (4) shows the configuration of the most efficient CAES system proposed.

In this system, at the time of compression, the heat rejected from the hot air in the first series of heat exchangers (HT1) is stored in the hot heat storage tank (Hot). In expansion time, when air is reclaimed for producing power, the hot water from this storage tank (Hot) warms up the high pressure air stream entering the turbines employing the second heat exchanger group (HT2). The cooled water, then, comes back to the cold storage tank (Cold). Auxiliary heaters are employed to produce the extra heat required before the expansion process.

In such system, efficiencies up to 80% are achievable. Note that the number of compressor and turbine stages could be defined with a trade off on the best energy performance of the CAES; however, it was shown in [33] that the most efficient performance can be obtained by a CAES including 5 stage compressor and 5 stage expander.

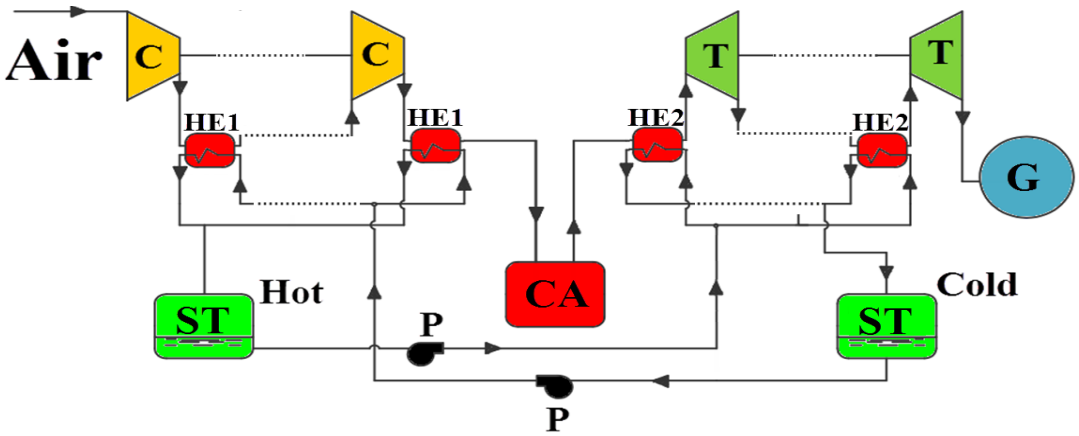

Figure 4 The optimum CAES system configuration; C: Compressor, HE1: The first group of heat exchangers, ST: Storage tank, CA: Cavern, T: Turbine, HE2: The second group of heat exchangers, P: Pump, G: Generator

(b) CAES Formulation

According to the operation principle of CAES system, there are two working stages. The first one is when there is extra electricity available. In this stage, this electricity is used to compress environment air employing the compressor set. The first group of heat exchangers is used here to collect the heat along with the air after each step of compression. This heat is, then, stored in a huge enough storage tank containing working fluid (mainly, water). In the second stage, when there is power shortage in PV plant production, the air is reclaimed from the cavern and after being warmed up through the second group of heat exchangers as well as the auxiliary air heater enters the expanders. The generator, finally, produces electricity.

For analyzing such a system, as figure (5) shows, three separate control volumes could be specified. For the first control volume in figure (5), as the compressor set total work ($\dot{W}_C$) is a functional of the available extra electricity, therefore, this parameter can be given by:

$$\dot{W}_C = P_E \times \eta_C \tag{4}$$

In which, P_E and η_C refer to the amount of extra power available and compressor overall efficiency respectively. Note as high mass flow rate and high pressure is required in the CAES system, centrifugal compressors are chosen to be employed in this work [35].

The value given by equation 4 is the total work of compressor set. For having the air mass flow rate through the compressor set, the work done by each compressor should be calculated separately. The previous study in this area shows that the efficiency of a centrifugal air compressor (η_C) can be given by [36]:

$$\eta_C = 1 - \left[0.04 + \frac{\beta' - 1}{150}\right] \tag{5}$$

Where, β' is the compressor compression ratio. Having compressor efficiency, one can easily calculate the specific work of compressor ($w_{C\text{-}act}$) with simple thermodynamic correlations. Then, for calculating this equation trial and train solution is required. Having all the compressors works, one can calculate the total air mass flow rate ($\dot{m}_C$) as:

$$\dot{m}_C = \frac{\dot{W}_C}{\sum w_{C\text{-}act}} \tag{6}$$

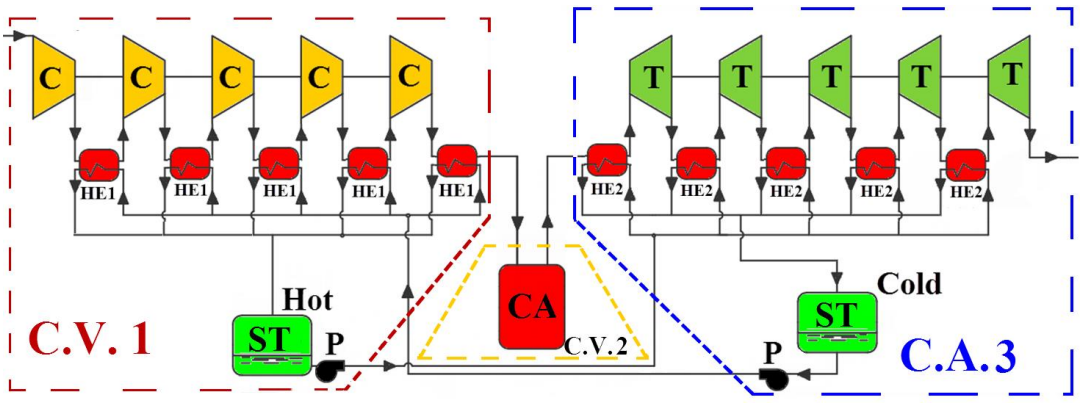

Figure 5 The CAES system separate control volumes

It bears mentioning that inlet air temperature is only known for the first compressor, which is equal to the ambient temperature. For calculating the other compressors inlet temperatures, energy balance on the first group of heat exchangers should be done simultaneously. The rate of heat transfer in the co-axial heat exchangers could be given by:

$$q = U \cdot A \cdot \Delta T_{lm} \tag{7}$$

Where, U, A and ΔT_{lm} are overall heat transfer coefficient, heat transfer area and logarithmic temperature difference respectively. Unlike the water flow that is laminar in the heat exchanger, due to the high mass flow rate of air through the heat exchangers, the air flow is always turbulent. Therefore, the overall heat transfer coefficient is given by:

$$U = \frac{1}{1/h_a + 1/h_W}; \qquad h_a = 0.023 \times Re_a^{0.8} \times Pr_a^{0.4} \times k_a/D_i; \qquad h_W = (4.63 \times k_W)/D_h \tag{8}$$

In these equations, h_a, h_W, Re_a, Pr_a, k_a, k_w, D_i and D_h are convective heat transfer coefficients for air and water, Reynolds and Prandtl numbers for air, thermal conductivity for air and water, internal diameter of the inner tube and hydraulic diameter for the outer tube, respectively. Logarithmic temperature difference in the heat exchanger is also given by:

$$\Delta T_{lm} = \frac{(T_{i-a} - T_{i-W}) - (T_{e-a} - T_{e-W})}{Ln\left(\frac{(T_{i-a} - T_{i-W})}{(T_{e-a} - T_{e-W})}\right)} \tag{9}$$

Finally, the air outlet temperature from each stage of heat exchanger (T_{e-a}), which is also equal to the inlet compressor temperature in the next stage, as well as the outlet water temperature (T_{e-W}) could be given by:

$$T_{e-a} = T_{i-a}(1-\varepsilon) + \varepsilon \cdot T_{i-W} \tag{10}$$

$$T_{e-W} = \frac{\varepsilon \cdot \dot{m}_a \cdot C_{p-a} \cdot (T_{i-a} - T_{i-W})}{\dot{m}_W \cdot C_{p-W}} + T_{i-W} \tag{11}$$

In the above equation, T_{i-W} is always considered equal to the ambient temperature. Also, ε in the above equations is the heat exchanger effectiveness and is calculated as:

$$\varepsilon = \frac{UA/C_{min}}{1 + UA/C_{min}}; \quad C_{min} = \dot{m}_a \cdot c_{p-a} \tag{12}$$

As can be seen, for implementing the above formulation, first of all, the specific compressor work in each stage should be known. This parameter is a functional of compressor inlet temperature. For calculating compressors inlet temperatures the heat exchangers effectiveness which is a functional of air mass flow rate should be known. Therefore, for calculating this formulation series, trial and train solution should be taken. Finally, implementing the mass conservation law and the first law of thermodynamics on the storage tank, one has:

$$m_{sth}^{\lambda+1} = m_{sth}^{\lambda} + \left(\sum \dot{m}_i - \sum \dot{m}_e\right)^{\lambda} \cdot \Delta t \tag{13}$$

$$T_{sth}^{\lambda+1} = \frac{\left(\sum \dot{m}_i \, c_W \, T_i - \sum \dot{m}_e \, c_W \, T_e\right)^{\lambda} \Delta t + m_{sth}^{\lambda} \cdot c_W \cdot T_{sth}^{\lambda}}{m_{sth}^{\lambda+1} \cdot c_W} \tag{14}$$

Where, c_W, m_{sth} and T_{sth} are water specific heat, the mass and temperature of water in the hot storage tank respectively. The superscriptions λ and λ+1 also count the system working time steps. For the cavern, as the second control volume in the CAES system, the mass conservation law could be implemented as below:

$$m_{ca}^{\lambda+1} = m_{ca}^{\lambda} + \left(\sum \dot{m}_i - \sum \dot{m}_e\right)_{ca}^{\lambda} \cdot \Delta t \tag{15}$$

Where, m_{ca} is the mass of air in the cavern in each moment. Having the mass of air in the cavern and considering air as an ideal gas, one can calculate the air pressure in the cavern (P_{ca}) as:

$$P_{ca} = \frac{m_{ca} \cdot R \cdot T_{ca}}{V_{ca}} \tag{16}$$

In this equation, V_{ca} is the cavern volume and should be defined considering the maximum pressure allowable in the system as well as the maximum daily available extra electricity throughout the year. T_{ca} is also the cavern temperature and is always considered to be equal to ambient temperature.

In the third control volume, the turbine set total work ($\dot{W}_T$) depends on the amount of auxiliary electricity required ($P_{E\text{-}G}$).

$$\dot{W}_T = \frac{P_{E-G}}{\eta_{T-G}} \tag{17}$$

Where, $\eta_{T\text{-}G}$ is the turbo-generator set overall efficiency. Considering an isentropic process for the turbine, first, isentropic outlet temperature and subsequently, isentropic work of each turbine is simply calculated, the actual work of turbine ($w_{T\text{-}act}$) and actual outlet temperature (T_e) could be given. Just the same as the first control volume, iterative solution is required for calculating the accurate value of T_e. The total air mass flow rate through the turbine set can be given by:

$$\dot{m}_T = \frac{\dot{W}_T}{\sum w_{T-act}} \tag{18}$$

The second group of heat exchangers should also be analyzed one by one. For this objective, equations 7 to 12 could be employed again. Here also trial and train solution is necessary for obtaining the accurate values of turbine set total mass flow rate, turbines inlet and outlet temperatures, individual turbines works and the temperature of water outgoing from each stage of heat exchanger. Equations 13 and 14 could be re-employed for the cold storage tank as well. It is noteworthy here that the operating fluid in the system is water for which boiling temperature is 373 K. On the other hand, the air must be heated up to higher temperatures before entering the expanders. Therefore, auxiliary heater is required to warm the stream up to the desired temperature. The amount of fuel ($\dot{V}_f$) required to be burnt by this heater to provide the required heat ($\dot{Q}_a$) could be given by:

$$\dot{V}_f = \frac{\dot{Q}_a}{LHV \cdot \eta_h} \tag{19}$$

Where, LHV and η_h are lover heating value of the fuel (here gas oil) and the heater thermal efficiency (assumed to be 50%), respectively [17].

Note that for compression step, the equations associated with the first and the second control volumes should be solved at the same time. On the other hand, at the time of electricity generation, the equations related to the second and the third control volumes must be solved simultaneously.

4 The Proposed Configuration

In this section, the details of the proposed system, i.e. the PV farm accompanying with a CAES unit is presented. Figure (6) shows the suggested system schematic.

The PV plant produces electricity during sunshine hours. The contract between the plant managers and grid authorities indicates how much electricity is supposed to be sold to the grid at each moment. This selling pattern should be specified in advance. Current power purchase agreements between electric grid managers and PV plants stipulate that ramps above 10% of the value indicated in the contract result in financial penalties for the power producers.

Therefore, the selling pattern should be so selected that not only the maximum possible electricity is sold to the grid, but financial penalties for the power plant are also minimized. With this situation, there is certainly some periods during which the PV plant electricity production exceeds the instantaneous power required and also some periods in which the solar irradiation ramps cause the PV plant to not be able to cover the selling pattern.

In the proposed system, according to the figure, during extra electricity production times, the excessive power is used to run the compressors in the CAES system to produce high pressure compressed air. This compressed air is, then, utilized to offset the shortage of electricity produced by the PV plant when solar ramps occur.

As the capacity of the CAES system is constant and, on the other hand, the daily available solar energy is variable, some amount of compressed air may remain in the cavern. A portion of this extra air is used to produce power at peak consumption hours (early night hours) in which the electricity price is even more relative to daily times and the remaining portion is kept in the system to offset electricity shortage in early hours of the upcoming day.

There may also be some days in which the amounts of solar ramps are so high that the stored compressed air cannot offset all the electricity shortages during the day and consequently, the PV plant will be penalized. Therefore, one must trade off to find the most efficient selling electricity pattern economically. As this work doesn't include economic aspects, just as a sample, the selling pattern of the plant is considered equal to 80% of the monthly average actual instantaneous solar irradiation in Caico. This pattern will be discussed in the results section. As it was explained before, the PV plant is supposed to be designed to provide daily-averaged 50 MW electricity. For a PV plant with such capacity in Caico, 388600 m^2 PV cell made of silicon crystalline (monocrystalline) is required [37].

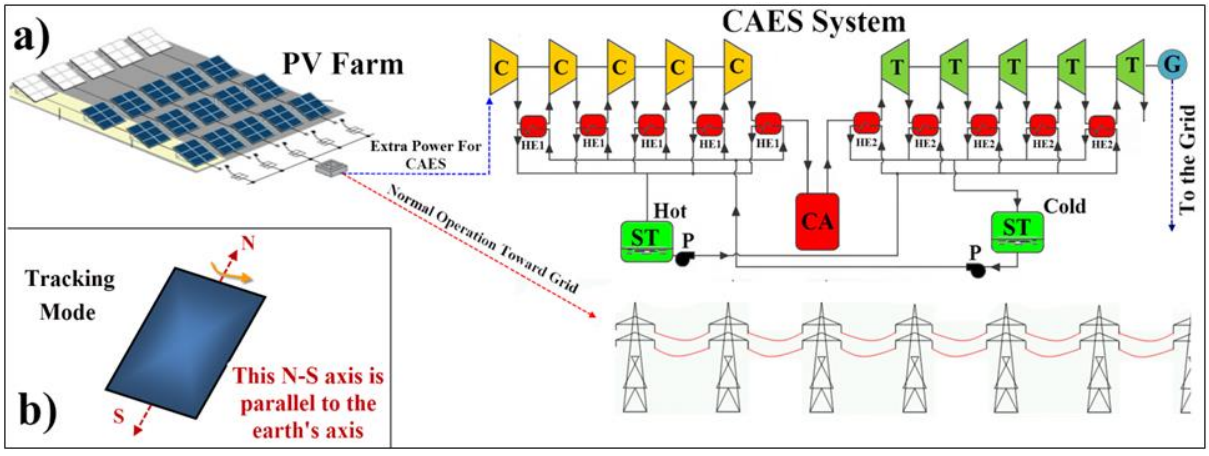

Figure 6 a) The proposed system schematic; b) the tracking mode schematic

In the CAES system in this work, the volume of the cavern is so selected that maximum pressure in cavern doesn't exceed 80 bar. Clearly, in multiple stage compressors and expanders depending on the cavern pressure the devices should change from parallel to series or reverse. The compression ratio ($\beta' = P_e/P_i$) in each stage of compressor is almost 2.9, just the same as the expansion ratio of expanders ($\beta'' = P_i/P_e$). The numbers of stages in compression and expansion procedures are recommended to be 5 [33]. In such a CAES system, the arrangement of compressors and turbines should change according to Ref. [33].
In addition, the CAES components capacity selection is done based on the maximum extra energy available (for the Compression unit) as well as the maximum electricity shortage that the system should offset (for the expansion unit).

5 Results and Discussion

In this section, the results of the analysis accomplished on the performance of the proposed plant are presented. The first required information for simulating the plant and the CAES system is the local average sunny hours of the day in each month and the environment temperature. Note that no weather station is located in Caico. The closest station to Caico is Natal station (with very similar climate conditions to Caico) and the most recent data by this station is for (2012). Therefore, the weather data released by Natal station in (2012) are used in the simulation procedure of this work. Figure (7) shows the total monthly sunny hours in Natal. According to the figure, the sunniest month over the year is November by almost 280 hours whereas April and June are the least sunny months by about 175 hours.
Figure (8) shows the environment temperature in Natal in (2012).

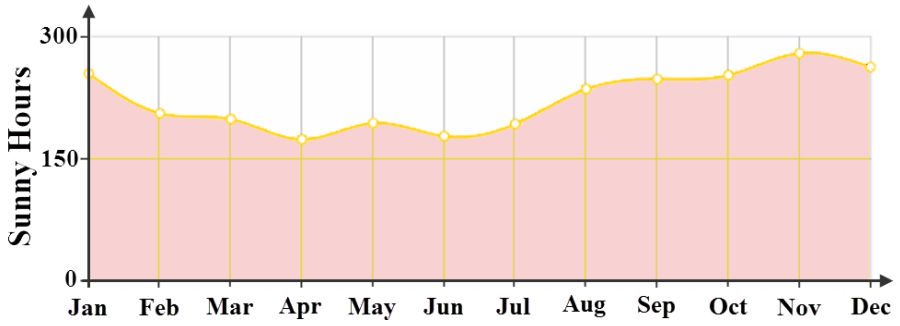

Figure 7 Total monthly sunny hours in Natal in (2012)

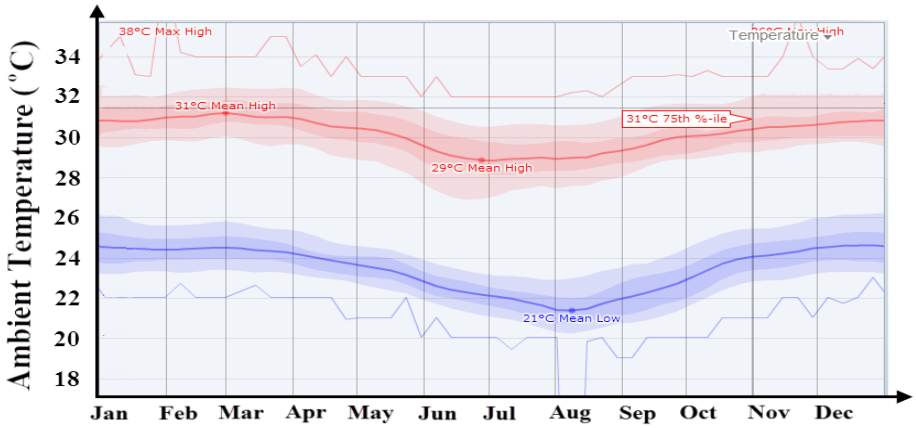

Figure 8 Ambient temperature in Natal in (2012)

Expectedly, as Brazil is located in the south hemisphere, January and February are the warmest months of the year while the coldest period of the year occur from July to August.
Figure (9) shows the average annual-hourly solar irradiation received by various types of tracking modes. Expectedly, the best tracking mode is dual axis tracking. However, this type of tracker is extremely costly due to the difficulties in manufacturing and designing stage.
On the other hand, among single axis rotator trackers, the best performance belongs to the surface that rotates around north-south axis parallel to the earth's axis. Therefore, this type of tracker is employed in the simulation of the PV plant in this work.
Figure (10) also shows the superiority of this mode of tracking relative to the other single axis rotating trackers in the form of total annual achievable solar irradiation. Note that figure (9) and (10) are resulted from the clear sky model while the actual data are certainly different due to the effects of clouds and other effective factors.

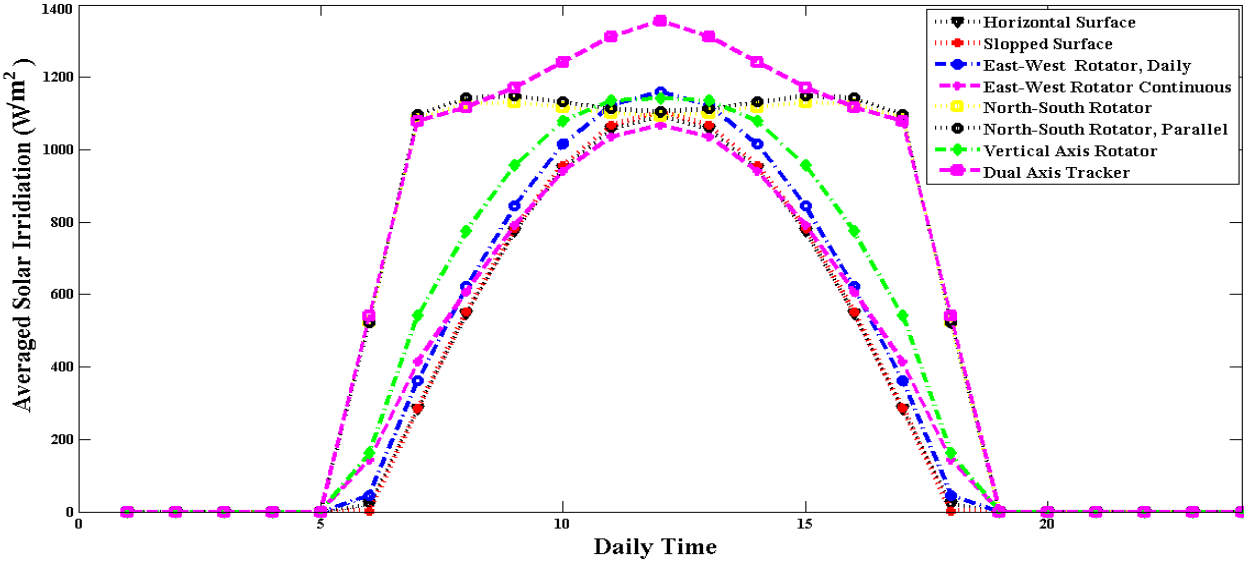

Figure 9 Annual-hourly averaged solar irradiation theoretically receivable by various tracking modes in Natal

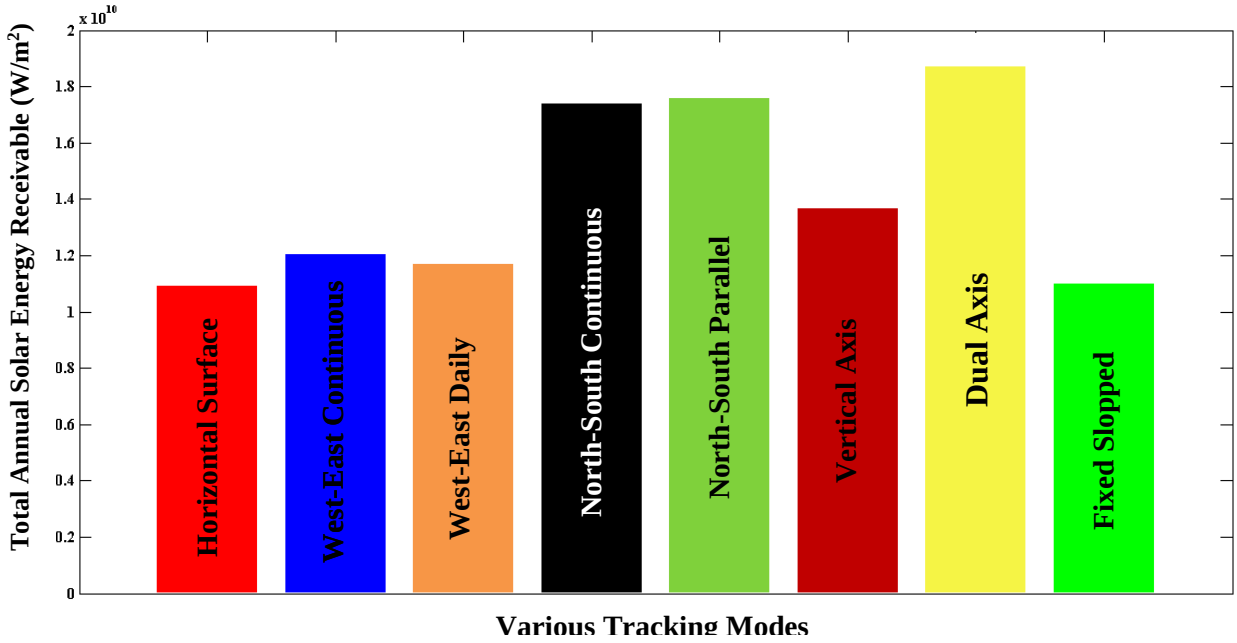

Figure 10 Total annual solar irradiation in various tracking modes by a surface with 1 m^2 area in Natal in (2012)

Figure (11) shows the actual solar irradiation on a horizontal surface recorded in Natal in (2012). Having the actual solar irradiation on a horizontal surface and calculating the amount of solar irradiation on a surface rotating about north-south axis parallel to the earth's axis by implementing the clear sky model, one could estimate the actual solar irritation receivable by this type of tracking surface. Figure (12) shows the monthly-instantaneously averaged solar irradiation theoretically and actually available in Natal when the tracking system is utilized. According to the figure, October and November have the maximum solar irradiation while June has the minimum amount of solar energy.

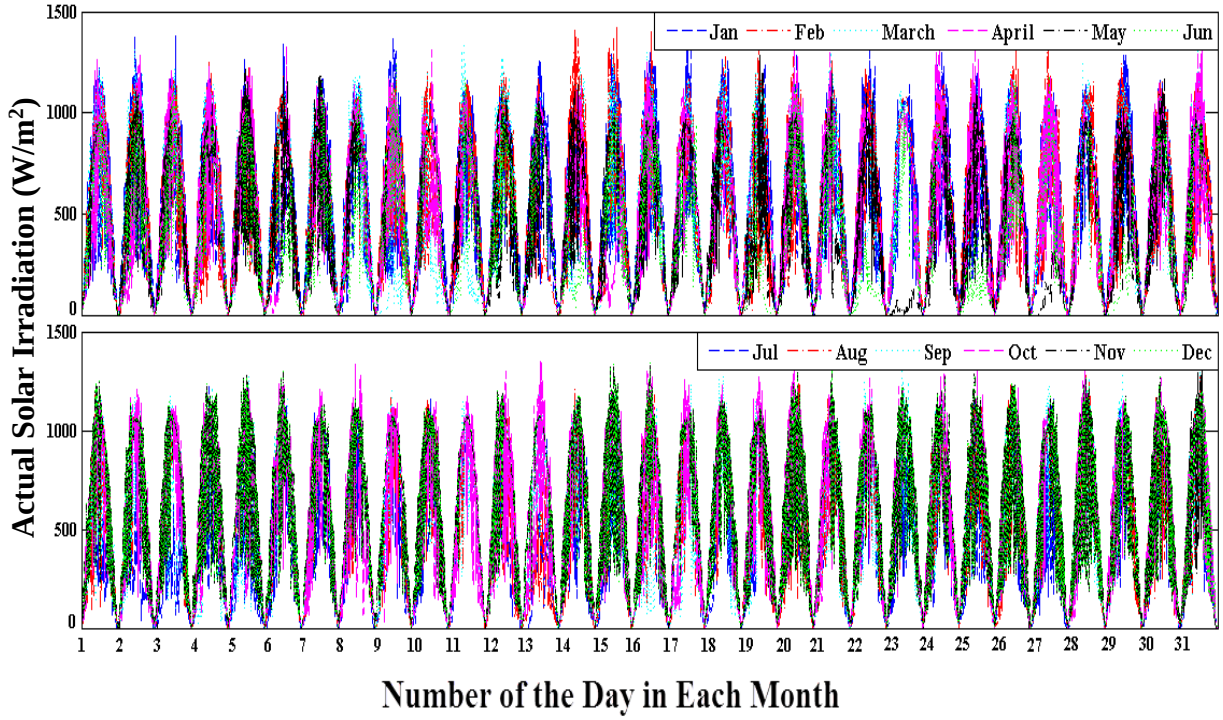

Figure 11 Actual Solar Irradiation on a horizontal surface with 1 m^2 area in Natal in (2012)

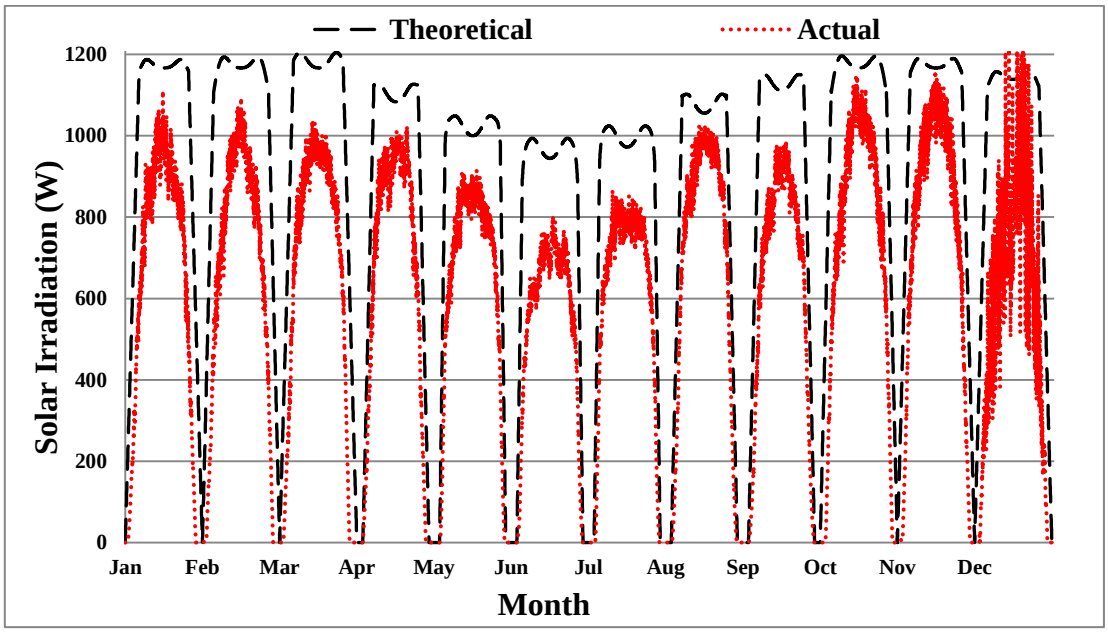

Figure 12 Instantaneously-monthly averaged actual and theoretical solar energy on the tracking surface with 1 m^2 area in Natal

As it was explained before, the capacity of the PV plant is so chosen that it averagely produces 50 MW electricity during the day. Therefore, the annual-daily averaged actual solar irradiation should be calculated. By averaging over the year, the instantaneously-yearly actual solar irradiation on the tracking surface from 6 am to 6 pm is calculated to be 688 W/m^2. Considering the utilized PV cells efficiency (19.3%) and the overall ground mounted PV cell modules efficiency (80% of the efficiency of an individual cell [38]), 132.8 W/m^2 electricity is producible averagely. Therefore, 470632 m^2 PV cells are required for the power plant. Figure (13) shows the monthly-instantaneously averaged electricity producible by the power plant for the first and second six months of the year respectively.

According to the figure it can be claimed that the PV plant capacity is 85 MWp which is produced in November at noon. As the figure shows, the least electricity is produced in June and October and November are responsible to produce the maximum amount of electricity. As can be seen, the real time producible electricity given by these graphs are not predictable. By curve fitting on these graphs, time dependent functions could be obtained by which the monthly-instantaneously averaged producible electricity could be estimated.

The electricity selling pattern of the PV plant, in this work, is defined 80% of the value given by these functions for each month. In this case, the average daily vendible electricity to the grid in each month will be according to figure (14). As can be seen, the results given by this figure are compatible with the results given in figure (13) so that the minimum electricity is sold in June with average daily 41.4 MWh and the maximum electricity is sold in November with the value of 60.7 MWh.

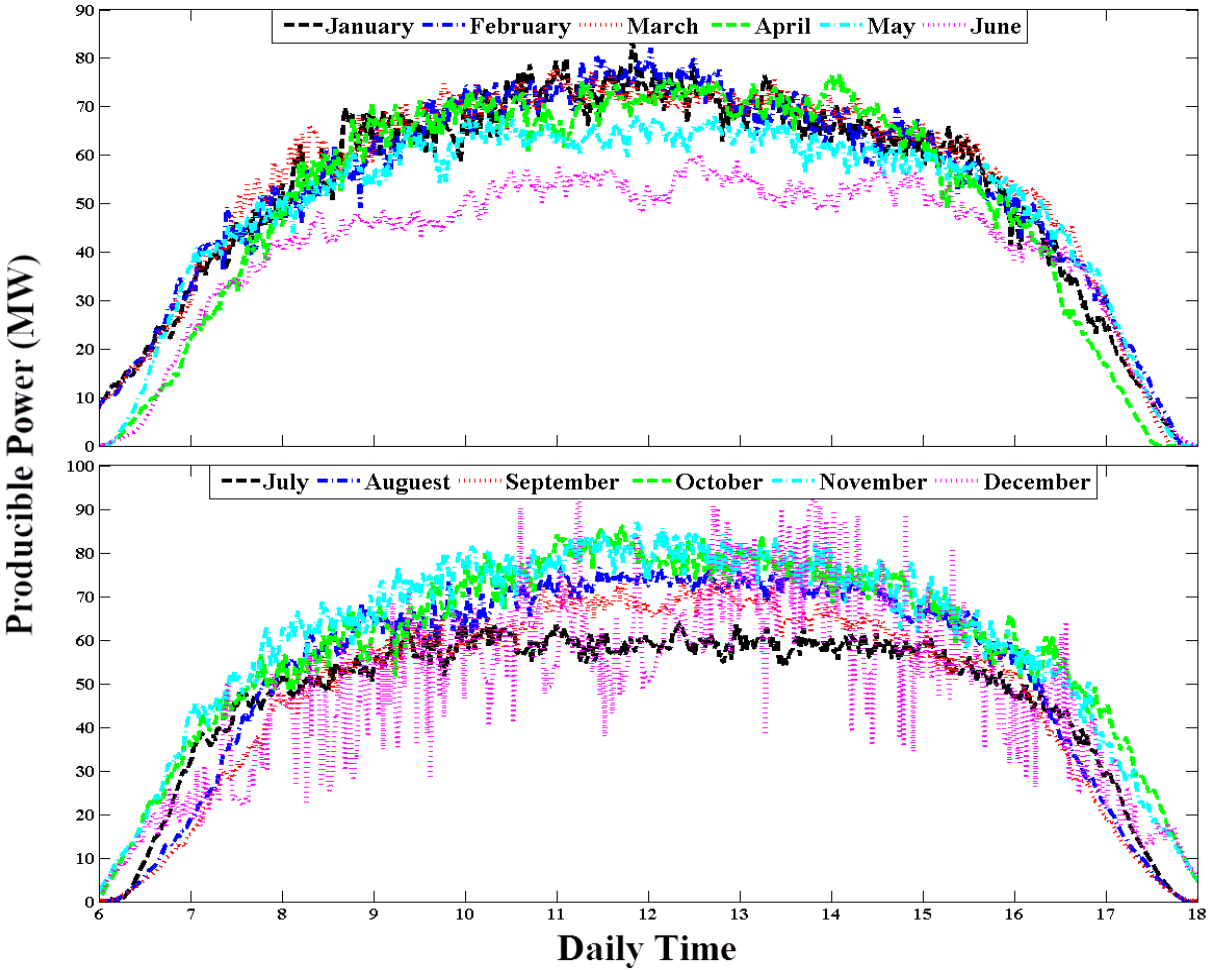

Figure 13 Instantaneously-monthly averaged actual producible electricity by the power plant

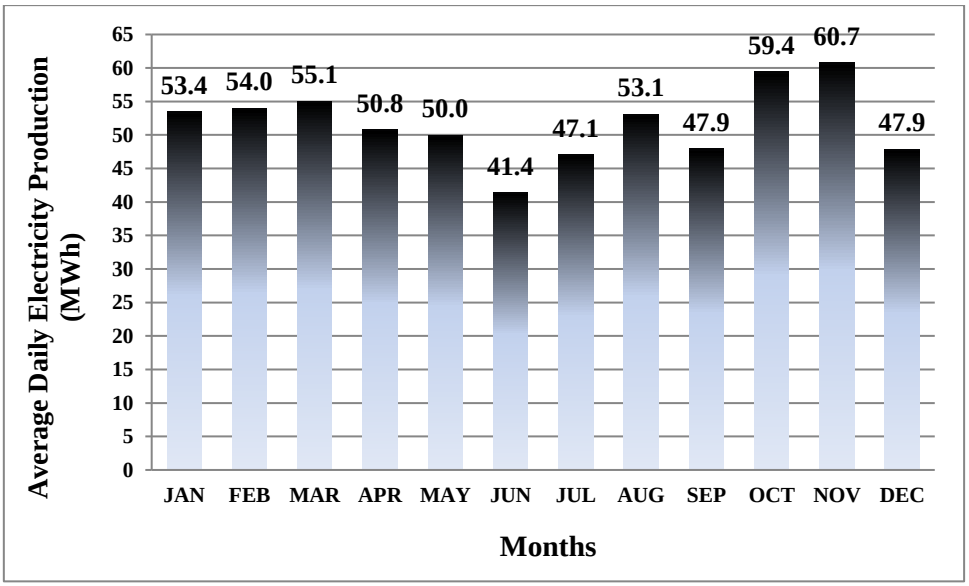

Figure 14 Daily averaged electricity salable to the grid in each month

In fact, the selling pattern is totally an economic issue and specialized analysis is required for defining this pattern. However, for showing the performance and effectiveness of the CAES system on the PV plant operational condition assuming a sample selling pattern seems to be inevitable. Even if anther selling pattern is found to not be the most economically efficient pattern, the simulation process doesn't affect and the results only simply change by varying the selling pattern.

Note that the simulation is done for all days of the year; however, for the sake of simplicity in showing the simulation results, the detailed results for only a few sample days of the year are presented.

Figure (15) shows the cavern pressure during the operational conditions of the CAES system with the opted volume for five sample days. These days were opted intentionally so that the variations of air pressure in the cavern could be shown in all possible cases from very sunny to very cloudy days.

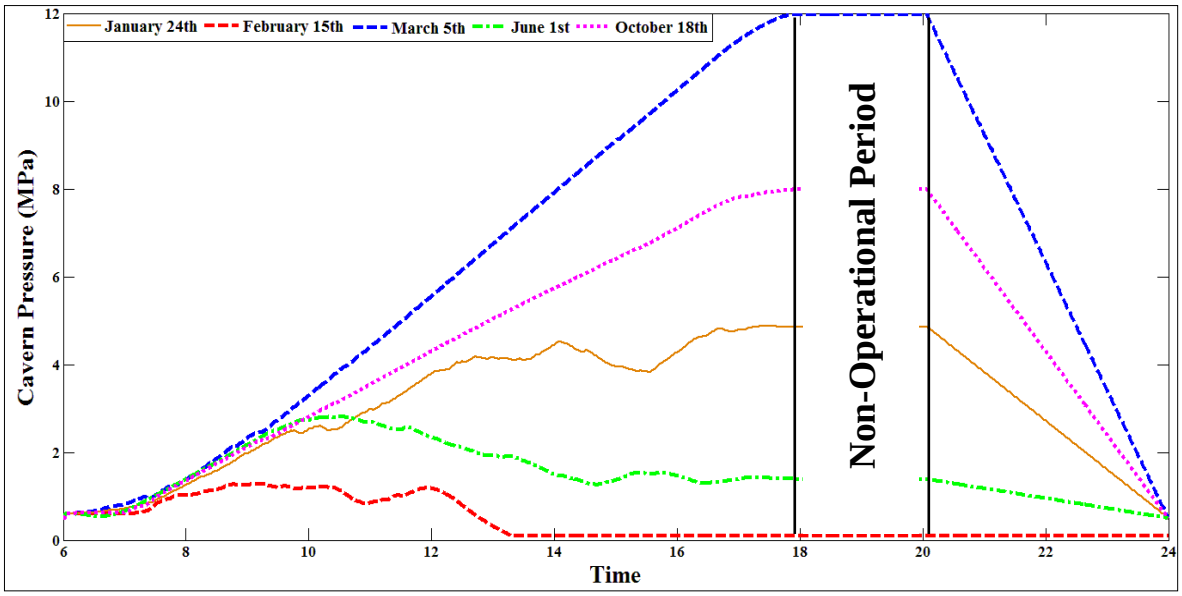

Figure 15 Cavern pressure variations during operational condition of the CAES system during five sample days

As it was mentioned, if there is still compressed air in the cavern at the end of the day, it is used to produce power at peak consumption period for 4 hours (from 8 pm to 12 pm) so much so that the cavern pressure decreases to 5 bar. This amount of air remains in the cavern in order to offset the ramps during early daily hours of the upcoming day. According to the figure, in February 15th, the sky is so cloudy that the PV farm could not support the CAES system that much and as a result, not much compressed air is produced during the day. In a sharp contrast, in March 5th, the PV farm produces much extra power and the CAES system could produce 100000 m^3 compressed air with 120 bar pressure at the end of the day. As solar ramps during the day had been trifle, this air is used to generate peak consumption period power. At the end of the day, obviously, the cavern pressure in all cases reduces to 5 bar, but in February 15th in which the cavern pressure is 0 bar (gauge pressure). Note that the cavern pressure is obviously a functional of the cavern volume. The cavern volume is considered to be 100000 m^3. With this volume of the cavern, its pressure doesn't exceed 120 bar over the year. It also bears mentioning that the cavern pressure decreases linearly at night while the CAES system produces peak consumption period electricity.

Figure (16) shows the total air mass flow rate compressed by the compressor set during these five days. Expectedly, during the days in which there is more extra power available to be used by the compressor set, compressed air with higher mass flow rates could be generated. According to the figure, the compressor set only works during the day (from 6 am to 6 pm).

On the other hand, in addition to the daily time during which the turbine set is used to offset power ramps in the PV plant, it could also be employed to generate peak period power from 8 pm to 24 pm. Figure (17) shows the mass flow rate of air flowing through the expanders. According to the figure, during peak consumption period, the air mass flow rate is constant. It is due to the system design pattern based on which the extra compressed air remaining in the cavern is supposed to produce constant amount of power for 4 hours. Naturally, higher value of air mass flow rate during this period means that more compressed air has been produced and fewer ramps occurred during the day.

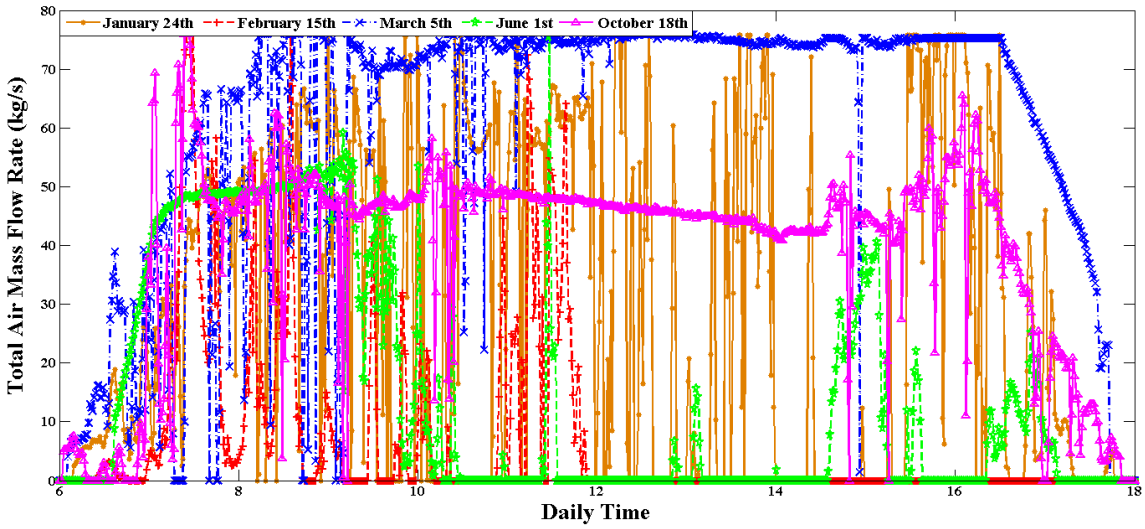

Figure 16 Compressed air mass flow rate during different days

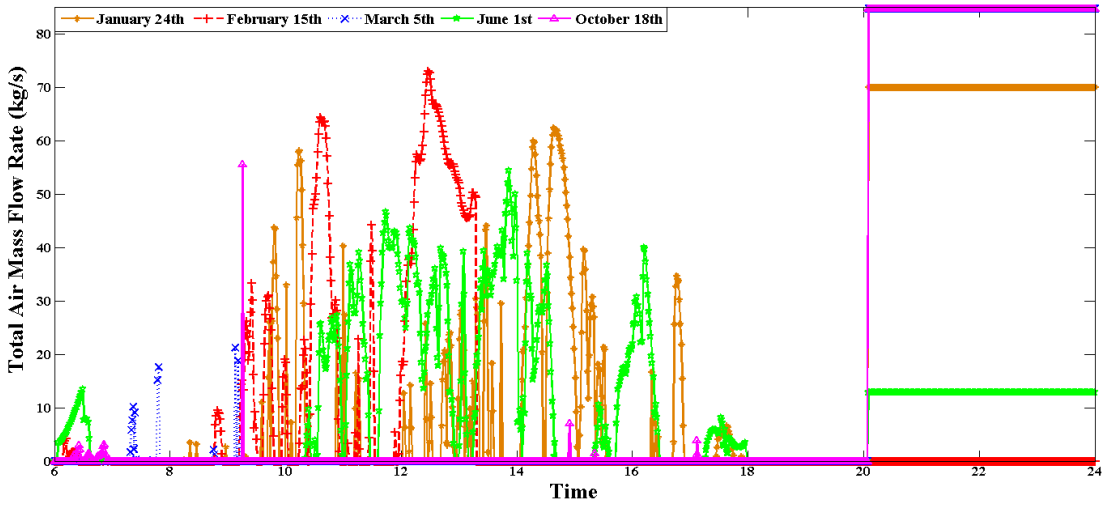

Figure 17 Expanding air mass flow rate during different days

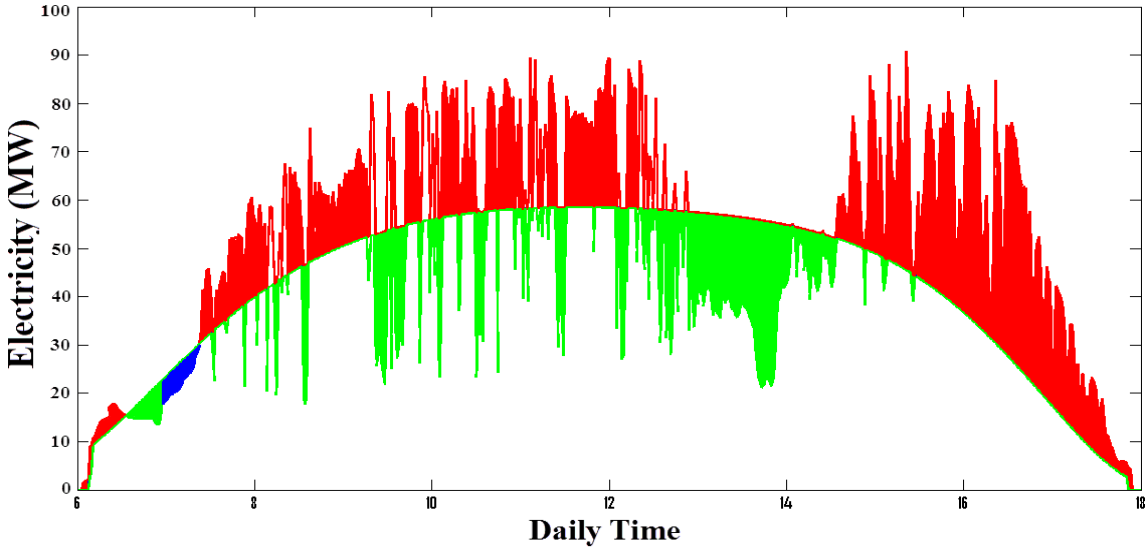

Figure 18 The CAES system effects on the performance of the PV plant in a sample day

As in the monthly averaged solar irradiation the intensity of the sudden solar ramps could not be well illustrated, this presentation format doesn't seem suitable for showing the turbine set total work. Therefore, figure (18) shows the CAES system effects for a sample day (January 2nd) over the year. In this figure, the turbine set work is clearly observable. According to the figure, the green spaces represent the times in which the turbo-generator in the CAES system offset the electricity shortage of the plant.

Evidently, the red space is where there is extra electricity available and the compressors produce compressed air employing this electricity. On the other hand, the blue space is the time when the CAES system is not able to offset electricity shortage and based on the mutual agreement between the grid managers and the plant, there will be financial penalty for the plant, though this area is so small in comparison with the electricity sold to the grid.

To assess the overall annual effect of the CAES system on the performance of the PV plant, figure (19) shows the total annual stored energy, the total annual electricity shortage compensated by the CAES system, the amount of electricity that the CAES system can produce for selling at peak consumption hours as well as the total amount of electricity shortage remained in the system for which the power plant is penalized financially.

Note that from the total stored energy in each day 20 MWh is kept in the CAES system to offset the electricity shortage of the early daily hours of the upcoming day and the remaining portion is used to produce peak electricity consumption period. According to the figure, 16024 MWh electricity shortage of the PV plant is offset by the CAES system. On the other hand, 35077 MWh nightly electricity is produced by the CAES system. The total annual electricity shortage remained in the system for which the plant is penalized is 1515 MWh which is a very satisfactory result considering the oscillatory nature of solar electricity.

Finally, figure (20) shows the amount of total monthly fuel (gasoil with LHV=38774.4 MJ/m^3) required to provide the auxiliary heat required for heating the compressed air entering the expanders. The values in this figure are in direct relation with the amount of total monthly the expander set work. The more solar ramps during the day, the more expanders need to be employed for producing power, and consequently, the more auxiliary heat is required. Evidently, the maximum fuel is consumed in January and the least fuel is burnt in June.

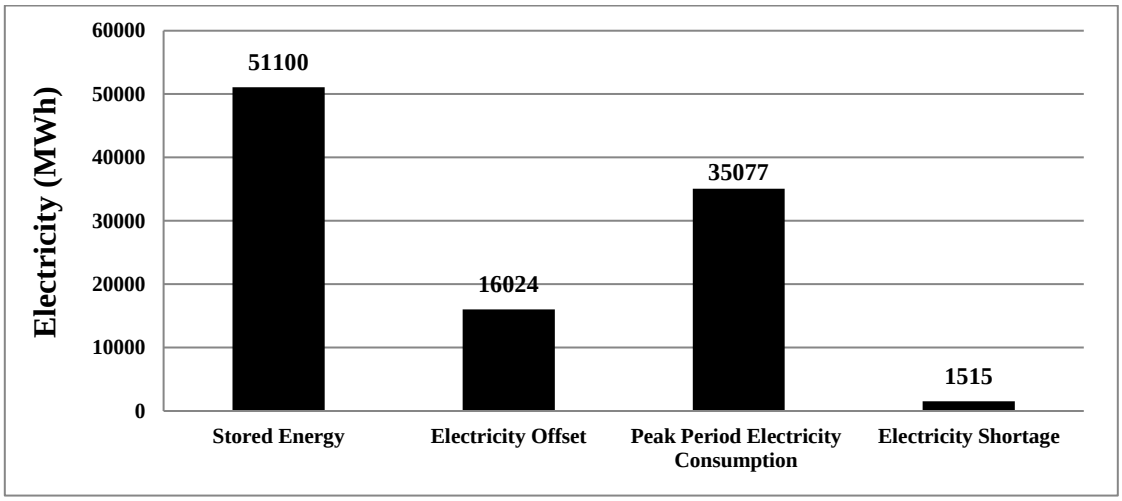

Figure 19 Overall annual statistics of the CAES system and PV plant

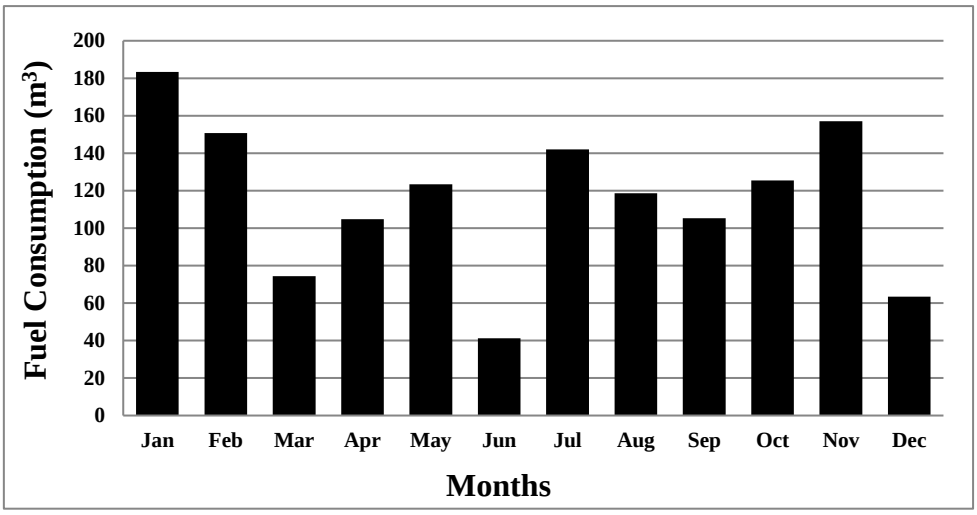

Figure 20 Total monthly fuel consumption of the auxiliary air heater in the CAES system

6 Conclusion

Brazil is one of the best countries in the world in terms of the amount of receivable solar irradiation; however, there is still no active solar energy source power plant in this country yet. In this work, constructing a PV plant accompanying with a CAES system in the most appropriate location in the country is proposed and its performance is simulated and analyzed. The results of the simulation well prove the effectiveness of the CAES system on the performance of the PV plant under dynamic operational conditions.
These results actually demonstrate that the CAES system can efficiently increase the net annual benefit of power plant minimize the financial penalties of the power plant due to the intensive solar energy ramps. It also could easily be conceived that if the CAES system capacity is selected accurately, and the PV plant power sales strategy is defined properly, the CAES system can even have much more considerable effects of the power plant economic and energy performance. Regarding the results of the simulation accomplished in this work, the implementation of solar energy power plants equipped with CAES systems in the countries with high solar energy potential is highly recommended.

References

[1] Arabkoohsar, A., Farzaneh-Gord M., Deymi-Dashtebayaz M., Machado L., and Koury R. N. N., "Energy and Exergy Analysis of Natural Gas Pressure Reduction Points Equipped with Solar Heat and Controllable Heaters", Renewable Energy, Vol. 72, pp. 258-270, (2014).

[2] Khadidjaa, B., Drisa, K., Boubekerb, A., and Noureddinec, S., "Optimization of a Solar Tracker System for Photovoltaic Power Plants in Saharian Region, Example of Ouargla, Energy Procedia", Vol. 50, pp. 610–618, (2014).

[3] Thanaraka, P., and Sae-Eirb, K., "Economic Analysis of CO2 Emission Reduction from Large Scale Photovoltaic Power Plant in Thailand", Energy Procedia, Vol. 14, pp. 837–842, (2012).

[4] Brunton, S. L., Rowley C. W., and Kulkarni, S. R., "*Maximum Power Point Tracking for Photovoltaic Optimization using Extremum Seeking*", Princeton University, Princeton, (2005).

[5] Wenger, H.J., Schaefer, J., Rosenthal, A., Hammond, B., and Schlueter, L., "Decline of the Carrisa Plains PV Power Plant", Photovoltaic Specialists Conference, Las Vegas, USA, pp. 586-592, (1991).

[6] Mellit, A., Pavan, A. M., and Lughi, V., "Short-term Forecasting of Power Production in a Large-scale Photovoltaic Plant", Solar Energy, Vol. 105, pp. 401-413, (2014).

[7] http://energy.gov/articles/agua-caliente-worlds-largest-solar-photovoltaic-plant-helps-advance -americas-solar

[8] Botterud, A., "Chapter 11–Forecasting Renewable Energy for Grid Operations", Renewable Energy Integration, pp. 137-147, (2014).

[9] Diagne, M., David, M., Boland, J., Schmutz, N., and Lauret, P., "Post-processing of Solar Irradiance Forecasts from WRF Model at Reunion Island", Solar Energy, Vol. 105, pp. 99-108, (2014).

[10] Pavković, D., Hoić, M., Deur, J., and Petrić, J., "Energy Storage Systems Sizing Study for a High-altitude Wind Energy Application", Energy, Vol. 76, pp. 91-103, 1 November, (2014).

[11] Gadhamshetty, V., Gude, V. G., and Nirmalakhandan, N., "Thermal Energy Storage System for Energy Conservation and Water Desalination in Power Plants", Energy, Vol. 66, pp. 938-949, (2014).

[12] Rodrigues, E.M.G., Godina, R., Santos, S. F., Bizuayehu, A.W., Contreras, J., and Catalão, J. P. S., "Energy Storage Systems Supporting Increased Penetration of Renewable in Islanded Systems", Energy, Vol. 75, pp. 265-280, (2014).

[13] Breeze, P., *"Chapter 10-Power System Energy Storage Technologies"*, Power Generation Technologies (Second Edition), pp. 195-221, (2014).

[14] http://www.tractebelenergia.com.br/wps/portal/internet.

[15] eco-inov.com.br/blog/

[16] http://www.cpc.noaa.gov/products/JAWF_Monitoring/Brazil/index.shtml.

[17] Farzaneh-Gord, M., Arabkoohsar, A., Deymi-Dashtebayaz, M., and Farzaneh-Kord, V., "Feasibility of Accompanying Uncontrolled Linear Heater with Solar System in Natural Gas Pressure Drop Stations", Energy, Vol. 41, pp. 420-428, (2012).

[18] Farzaneh-Gord, M., Arabkoohsar, A., Rezaei, M., and Deymi-Dashtebayaz, M., "Feasibility of Employing Solar Energy in Natural Gas Pressure Drop Stations", Journal of the Energy Institute, Vol. 84, No. 3, pp. 165-173, (2011).

[19] Funari, F. L., "Sunshine Hours, Global Solar Radiation and Net Radiation in Brazil, São Paulo", Masters Essay for the Geography Division of the University of São Paulo, São Paulo, Brazil, (1983).

[20] Kalogirou, A. S., "Solar Thermal Collectors and Applications", Progress in Energy and Combustion Science, Vol. 30, pp. 231–295, (2004).

[21] Duffie, J. A., and Beckman, W. A., *"Solar Engineering of Thermal Processes"*, Second Edition, Willy & Sons, New York, (1991).

[22] Zekai, S., *"Solar Energy Fundamentals and Modelling Techniques*", 3rd Ed., Springer 180, London, (2008).

[23] Manor, A., and Katz, E. A., "Open-circuit Voltage of Organic Photovoltaics: Implications of the Generalized Einstein Relation for Disordered Semiconductors", Solar Energy Materials and Solar Cells, Vol. 97, pp. 132-138, (2012).

[24] Gu, X., Yu, X., Guo, K., Chen, L., Wang, D., and Yang, D., "Seed-assisted Cast Quasi-Single Crystalline Silicon for Photovoltaic Application: Towards High Efficiency and Low Cost Silicon Solar Cells, Solar Energy Materials and Solar Cells, Vol. 101, pp. 95-101, (2012).

[25] Neville, R. C., "Solar Energy Collector Orientation and Tracking Mode", Solar Energy, Vol. 20, No. 1, pp. 7-11, (1978).

[26] Yao, Y., Hu, Y., Gao, S., Yang, G., and Du, J., "A Multipurpose Dual-axis Solar Tracker with Two Tracking Strategies", Renewable Energy, Vol. 72, pp. 88-98, (2014).

[27] Raju, M., and Khaitan, S. K., "Modelling and Simulation of Compressed Air Storage in Caverns: A Case Study of the Huntorf Plant", Applied Energy, Vol. 89, No. 1, pp. 474-481, (2012).

[28] http://www.powersouth.com/mcintosh_power_plant/compressed_air_energy

[29] Schulte, R. H., Critelli, N., Holst, K., and Huff, G., "Lessons from Iowa: Development of a 270 Megawatt Compressed Air Energy Storage Project in Midwest Independent System Operator", A Study for the DOE Energy Storage Systems Program, Sandia Report, (2012).

[30] Kousksou, T., Bruel, P., Jamil, A., Rhafiki, T. E., and Zeraouli, Y., "Energy Storage: Applications and Challenges, Solar Energy Materials and Solar Cells", Vol. 120, Part A, pp. 59-80, (2014).

[31] Porto, M. P., Machado, L., and Koury, R. N. N., "An Alternative Solution Based on Compressed and Liquefied Air Storage Systems for Reducing Power Output Variability From PV Solar Farms, 22nd International Congress of Mechanical Engineering (COBEM), Ribeirão Preto, SP, Brazil, (2013).

[32] Safaei, H., Keith, D. W., and Hugo, R. J, "Compressed Air Energy Storage (CAES) with Compressors Distributed at Heat Loads to Enable Waste Heat Utilization", Applied Energy, Vol. 103, pp. 165-179, (2013).

[33] Grazzini, G., and Milazzo, A., "Thermodynamic Analysis of CAES/TES Systems for Renewable Energy Plants", Renewable Energy, Vol. 33, pp. 1998–2006, (2008).

[34] Wark, K., and Richards, D. E., *"Thermodynamics"*, 6th edition, Tom Casson, (1999).

[35] Meherwan, P. B., "6-Centrifugal Compressors", Gas Turbine Engineering Handbook, Fourth Edition, pp. 253-301, (2012).

[36] Li, W., "Simplified Steady-state Modeling for Variable Speed Compressor", Applied Thermal Engineering, Vol. 50, No. 1, pp. 318-326, (2013).

[37] http://www.e-tonsolar.com/upload/Datasheet-ETS6-3BB-Diagonal%20200_ 20111222 %281%29.pdf

Nomenclature

A	Heat transfer area	(m^2)
c_p	Specific thermal capacity	(kJ/kg.^oC)
D and d	diameter	(m)
G_{sc}	Solar Constant	(W/m^2)
h_a	Convective heat transfer coefficient of air	($W/m^2.K$)
h_W	Convective heat transfer coefficient of water	($W/m^2.K$)
I	Solar irradiation on a horizontal surface on the earth	($W/m^2.hr$)

I_b	Beam component of solar irradiation	($W/m^2.hr$)
I_d	Diffuse component of solar irradiation	($W/m^2.hr$)
I_o	Solar irradiation on a horizontal surface beyond the atmosphere	($W/m^2.hr$)
k	Thermal conductivity	($W/m.^oC$)
LHV	Lowering heating value	(kJ/kg)
m	Water mass in the heat exchanger	(kg)
$\dot{m}_C$	Total air mass flow rate	(kg/s)
P	Pressure	(kPa)
P_E	Extra power available for the CAES system	(MW)
P_{E-G}	Energy shortage in the system	(MW)
q	Heat transfer rate	(kW)
t	Time	(s)
T	Temperature	(^oC or K)
U	Overall heat transfer coefficient	($W/m^2.C$)
V	Volume	m^3
$\dot{V}$	Volume flow rate	(m^3/s)
w_{C-act}	Actual work of compressors	(kJ)
w_{T-act}	Actual work of compressors	(kJ)
$\dot{W}_c$	Compressor set total work	(kW)
$\dot{W}_T$	Turbine set total work	(kW)

Greek Symbols

φ	Latitude angle
δ	Inclination angle
ω	Hourly angle
β	Slop Angle
β'	Compression ratio
β''	Expansion ratio
ρ_g	Reflection solar irradiation coefficient
θ	Incident angle
θ_z	Zenith angle
γ	Surface azimuth angle
η_C	Compressor overall efficiency
η_{T-G}	Turbo generator efficiency
λ	Time step
ε	Heat exchanger effectiveness

Subscriptions

a	air
am	Ambient
b	Borehole
ca	Cavern
e	External
f	Fuel
i	Internal
T	Turbine
w	Water
h	heater

چکیده

استفاده از سلول های فتوولتاییک در طول سالیان گذشته در کاربردهای صنعتی و خانگی به سرعت توسعه یافته است. ساختن نیروگاه های فتوولتاییک یک تدبیر بسیار هوشمندانه برای تولید برق رایگان در ظرفیت های بالا می باشد، مخصوصا در کشورهایی که پتانسیل دریافت انرژی خورشیدی بالاتری دارند. در سوی دیگر، سیستم ذخیره هوای فشرده قبلاً به عنوان یک سیستم بسیار بهینه برای ذخیره انرژی معرفی گردیده است. در این پژوهش، احداث یک نیروگاه متصل به شبکه در مقیاس بزرگ که به یک سیستم ذخیره انرژی هوای فشرده مجهز می باشد در بهترین نقطه خاک برزیل پیشنهاد شده است. در مرحله اول، بهترین نقطه برای احداث این نیروگاه مشخص می گردد و سپس بهترین استراتژی تعقیب خورشید با درنظر گرفتن ملاحظات فنی و اقتصادی انتخاب می شود. سپس، سیستم ذخیره ساز انرژی خورشیدی طراحی می گردد. برای اثبات بهینه بودن سیستم پیشنهادی، عملکرد آن در طول یک سال کامل مورد ارزیابی قرار می گیرد.